

## FLOW FIELD ANALYSIS OF A TRAILING EDGE INTERNAL COOLING CHANNEL

A. Andreini, C. Bianchini

Department of Energy Engineering "Sergio Stecco"  
Via Santa Marta, 3 - 50139 Firenze, Italy  
Email: antonio.andreini@htc.de.unifi.it

A. Armellini, L. Casarsa

Department of Energy Technologies and Machinery  
Via delle Scienze 208 - 33100 Udine, Italy

### ABSTRACT

Internal blade cooling cavities show ever increasing geometrical complexity. Consequently, a deep insight on the flow behavior is mandatory for a reliable design, while trustworthy experimental databases are definitely needed to assess the reliability of numerical prediction tools.

Present contribution provides a detailed investigation of the flow field inside a modern internal cooling passage for turbine blade trailing edge. The investigation is carried out by coupling the results of accurate Particle Image Velocimetry (PIV) measurements and steady state CFD predictions.

The channel is characterized by an high aspect-ratio trapezoidal cross section of width and height that reduce progressively moving from blade hub to tip and trailing edge, respectively. The flow has a mixed radial-axial direction, it enters the channel at the blade hub, and it is discharged radially at the tip and along the trailing edge. In this latter exhaust section, 7 pedestals guarantee structural resistance and enhance the turbulent heat transfer.

The investigation is carried out at an engine representative Reynolds number of 20000 and for two values of the mass flow split between tip and trailing edge exhaust sections. 2D-PIV measurements were performed on several flow planes, carefully selected to allow a comprehensive reconstruction of the 3D flow field inside the passage. Three main aspects have been considered. The first one was the characterization of the flow field at the inlet, which represents the boundary condition for the numerical problem. The second objective was the definition of the mass flow distribution along the trailing edge slot and at the blade tip. Finally, highly spatially resolved measurements were performed inside the inter-pedestals passages. 3D flow separations and

horse-shoe vortex branches were observed on the downstream and upstream pedestals' surfaces, respectively.

In order to verify the accuracy of typical industrial CFD, a comparison of experimental flow field with numerical results obtained with both a commercial (Ansys® CFX®) and an in-house developed (open source toolbox OpenFOAM®) 3D RANS solver was performed. The accuracy of the commonly used  $k-\omega$  SST turbulence model to predict the extent of recirculating flows was investigated and discussed. Both codes provided satisfactory results showing also good confidence in the prediction of the complex 3D flow structures inside the inter pedestal passages.

### NOMENCLATURE

$D_h$	inlet hydraulic diameter	[mm]
$k$	turbulent kinetic energy	[m <sup>2</sup> /s <sup>2</sup> ]
$P$	data extraction line	
$q$	mass flow rate	[kg/s]
$Re$	Reynolds number $Re = \rho \cdot U_b \cdot D_h / \mu$	[-]
$U$	X velocity component	[m/s]
$U_b$	bulk velocity	[m/s]
$V$	Y velocity component	[m/s]
$vel$	Velocity magnitude	[m/s]
$W$	Z velocity component	[m/s]
$X$	quasi-radial coordinate	[m]
$Y$	axial coordinate	[m]
$Z$	quasi-tangential coordinate	[m]

### Greeks

$\alpha$	incidence angle $\alpha = -atan(U/V)$	[deg]
$\rho$	density	[kg/m <sup>3</sup> ]
$\mu$	dynamic viscosity	[kg/ms]

## Acronyms

<i>AR</i>	aspect ratio
<i>OF</i>	OpenFOAM
<i>PIV</i>	Particle Image Velocimetry
<i>RANS</i>	Reynolds Averaged Navier-Stokes

## Subscripts

<i>in</i>	relative to the inlet section
<i>RMS</i>	Root Mean Square
<i>te</i>	relative to the trailing section
<i>tip</i>	relative to the tip section

## INTRODUCTION

Today advances in aero-engine design are mainly driven by the requirement of higher thrust/weight ratios, reduction of fuel consumption and pollutant emissions. To achieve these challenging goals, manufacturers have generally increased the operating temperature, i.e. the turbine inlet temperature, that in turn has prompted them to use efficient cooling systems and thermal barrier coatings for the components that are subjected to high thermal loads. Even if sometimes driven by different requirements, an efficient blade cooling system is of course a primary design objective also in land-based gas turbines.

Among the engine components, the turbine blades trailing edge is one of the most critical, due to quite strict aerodynamic, thermal and structural constraints that oblige to use cooling channels characterized by high aspect-ratio cross sections, multiple exhausts and turbulators of various shapes. In particular, the exhaust slot at the trailing edge is often provided with elongated pin-fins, usually named pedestals, which enhance the turbulence level and guarantee the necessary blade structural solidity.

Most of the studies available in literature deal with cooling schemes normally used for the blades central body, i.e. square or rectangular rib-roughened channels, where the coolant flows along the main channel axis, eventually in multiple passages configuration. A limited number of different studies regarding advanced trailing edge cooling channels can be found in literature. Among them, Taslim et al. [1] presented a thermal analysis of the cooling performances of a ribbed radial channel with axial outlet through slots. Armellini et al. [2] and Coletti et al. [3] presented an exhaustive analysis of both the thermal and flow fields and a comparison of the experimental data with RANS numerical solutions in a channel of geometry comparable to that used in [1]. More recently, Coletti et al. [4] completed the thermal analysis with conjugate heat-transfer measurements. Geometries with cut-back have been investigated by Choi et al. [5] and by Cakan and Taslim [6], the latter both experimentally and numerically. Experimental investigations, mainly focused on the thermal aspects, conducted on cooling channels with shape and aspect ratio similar to the one of the present study can be found in Facchini et al. [7, 8] and provided with differently shaped ribs and pins. By means of liquid crystal thermography, they have performed

measurements of the wall thermal field in axial or axial-radial cooling flow configurations with different turbulence promoters (pedestals, ribs or pin-fins), placed just upstream of the trailing edge exhaust section. Such technique was later exploited also for extensive pin arrays and enclosed by a numerical campaign and flow field investigations [9]. A parallel analysis oriented at assessing the heat transfer performance of the same geometry at the same condition was performed experimentally by Bonanni et al. [10] and numerically by Bianchini et al. [11] also including the effect of rotation.

This paper aims at carefully investigating the flow field inside a wedge-shaped converging duct with seven pedestal that guides the coolant towards the trailing edge exit slot. In particular such relatively simple configuration with respect to previously studied similar geometries, was chosen as a suitable environment to obtain a basic characterization of the flow features associated to the turbulence promoters also expected in more complex discharge duct designs. Along with the axial redirection of the inlet radial flow, the present study takes into account the effect of the tip mass flow rate; for this purpose a closed tip condition was considered together with a blowing tip at ambient pressure. Flow conditions were fixed at  $Re = 20000$  in the feeding channel.

Detailed two-dimensional PIV measurements of the mean velocity distribution were acquired at several horizontal and vertical planes. A parallel numerical analysis, involving both the commercial CFD code CFX<sup>®</sup>11 and the open source toolbox OpenFOAM<sup>®</sup>, was performed with the aim of testing the prediction capabilities of steady-state RANS CFD codes against such an accurate experimental database. Results are hence compared and analysed qualitatively in terms of velocity magnitude two-dimensional maps and quantitatively on selected profiles extracted by such planes. Finally the mass flow rate discharged by each inter-pedestals passage was evaluated.

## EXPERIMENTAL APPARATUS AND PROCEDURE

### Test rig and geometries

The channel geometry is sketched in Fig.1-A. The main flow direction is radial (X axis), the coolant enters the passage at the blade hub and it is exhausted at both the tip and the trailing edge. The inlet section is rectangular ( $D_h = 58.18$  [mm]) and with high aspect-ratio ( $AR=7.25$ ), typical of the most recent cooling passages for blade trailing edges. The channel width reduces progressively when moving from hub to tip in order to ensure a proper flow distribution all along the trailing edge. This latter region, is characterized by a wedge shaped cross section and by the presence of seven elongated pedestals installed to promote flow turbulence and ensure structural solidity. At the end of the trailing edge, a short channel with rectangular cross section (having the same height of the channel but  $AR=3.625$ ) guides the flow towards the tip exhaust section, which is made of five equally spaced holes of 7 [mm] radius. With the aim of testing the accu-



surement window, 1000 samples have been acquired and then ensemble averaged to compute time averaged velocity fields and the related turbulent statistics. Due to the low acquisition frequency (4 [Hz]), the samples can be considered as statistically independent and in a number sufficiently high to guarantee the convergence of both first and second order statistics.

As PIV is a comparatively complicated experimental technique, there is no simple means available to check the accuracy of PIV measurements. Nevertheless, a careful analysis of the different sources of PIV errors was already performed by Casarsa and Giannattasio [15] with reference to a flow field similar to the present one (three-dimensional shearing flow). Following such analysis, an overall upper bound estimate of the uncertainty in the mean velocities turns out to be less than 2% (95% confidence level) in the most of the flow field, except for limited regions inside the recirculation bubbles affected by very low velocities and high fluctuations. Under the same assumptions, the maximum uncertainty in the estimate of the root mean square velocity fluctuations is 5%.

### Measurement planes and test conditions

The experiments have been performed at  $Re=20000$  defined on both bulk velocity ( $U_b$ ) and hydraulic diameter ( $D_h$ ) computed at the channel entry section. Constant ambient pressure is maintained at the channel outlets. It is important to notice that in real engine conditions such devices are subjected to a different pressure distribution (usually increasing from hub to tip) determined by the blade aerodynamics. In the present case, the choice to impose a constant pressure at the channel exhausts, is justified by the need to perform the analysis in a condition easy to be accurately reproduced both numerically and experimentally. However, it is reasonable to expect that the pressure boundary condition will not modify substantially the main flow features in case of moderate radial gradients. The assessment of the computational techniques under these simplified conditions would also provide efficient tools to perform simulations reproducing more realistic pressure distributions with an equivalent level of confidence in the results.

The flow planes selected for the PIV measurements are reported in Fig.1-B. The collected data allow to describe the global flow structures and to investigate the mass flow split between the different exhaust sections. Two horizontal planes  $xy$  are located at half channel height ( $xy1$ ) and at half height of the trailing edge exhaust section ( $xy2$ ). To investigate more in detail the inter-pedestals secondary structures, measurements have been acquired also in  $xy3$  and  $xy4$  planes which are parallel to the channel surfaces and 2 [mm] distant from them. Measurements along  $xz$  planes have been acquired at the channel inlet ( $xz\_in$ ), in planes  $xz1$  and  $xz2$  for a more detailed insight on the vortical structures around the pedestals and on the symmetry planes of the 5 jets ( $xz-F1, \dots, xz-F5$ ) to investigate the tip exhaust section.

The dotted lines ( $Pin\_xy$ ,  $Pin\_xz$ ,  $Pte1..3$ , and  $Ptip$  in Fig.1-B) give the locations where velocity profiles have been extracted for the data analysis reported in the following sections.

### NUMERICAL METHODOLOGY

Numerical simulations were conducted using both the commercial solver Ansys®CFX®11.0 and an in-house developed CFD solver based on the open-source toolbox for continuum mechanics called OpenFOAM®. Steady-state assumption and RANS turbulence modeling were exploited in order to reduce the cost of a reliable simulation up to an affordable dimension.

Concerning CFX®simulations the convective terms were discretized following the High Resolution scheme that is a bounded second order upwind scheme [16]. The in-house code differs from the previous solver mainly for the treatment of pressure momentum coupling, the choice of the algorithm however does not affect accuracy but only influences convergence rate: CFX®uses a coupled algorithm while the OpenFOAM®C++ library, implements finite volume discretization aimed at solving pressure and momentum in a segregated way [17, 18]. The system of compressible Navier-Stokes Equations is solved using a SIMPLE-like (Semi-Implicit Method for Pressure-Linked Equations) algorithm with a convective diffusive equation for the pressure correction to impose mass continuity considering density variation [19]. Convective schemes uses a second order upwind interpolation scheme based on the NVA (Normalized Variable Approach) known in literature as Self Filtered Central Differencing [20] blended with a first order upwind scheme exploiting a deferred approach, in such a manner accuracy of second order schemes is achieved maintaining stability properties typical of upwind schemes.

Turbulence was modeled in both codes by means of the  $k - \omega$  SST model. A different near wall treatment is implemented for the two computations: an hybrid near wall treatment in CFX®with square root blending [21] and a purely Low Reynolds implementation in OpenFOAM®. At an early stage of this research comparison between such Low-Reynolds treatment and the exponential blending [22] available for the OpenFOAM®code [23] was performed too, giving practically equal results. In the past such different wall function treatments proved to affect heat transfer predictions at least for less near wall refined computational grids [9].

All runs were conducted isothermal, assuming perfect gas behaviour and constant thermo-physical properties, the very low Mach expected permits such simplifications without any significant loss of accuracy.

The boundary conditions applied followed a classical scheme for incompressible and LowMach number flow simulations, as sketched in Fig.2 where an overview of the computational domain is given. A velocity distribution is imposed at the inlet surface while ambient static pressure (101325 [Pa]) is main-

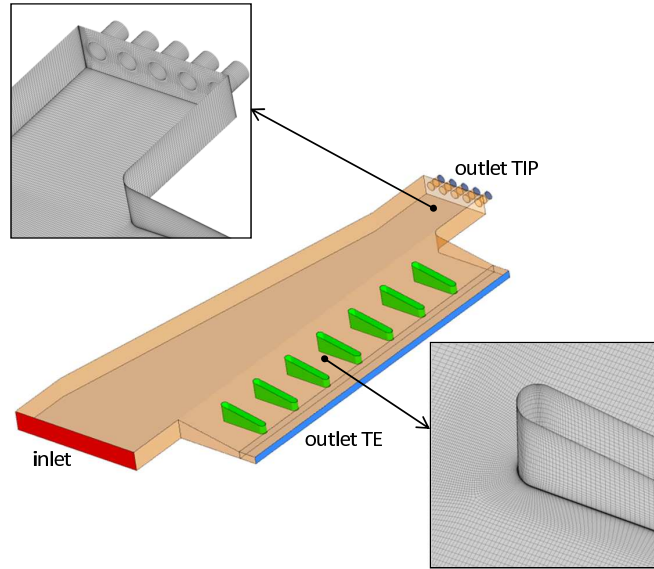


**FIGURE 2. Overview of computational domain and local mesh details**

tained at the outlets. The inlet velocity map was obtained from the experimental campaign as explained in the following section.

The multiblock structured mesh in use is composed by  $6.2 \cdot 10^6$  hexahedral cells. A grid independence study was performed starting from a first trial mesh consisting of 3.5 million cells. A preliminary run confirmed that the highest disagreement between computations and experiments was located in the first inter-pedestal duct and in the structures developing around the pedestal leading edges. As a consequence efforts were directed in refining those zones as long as the velocity profile at the entrance of the trailing edge duct was mesh independent all through the radial development.

Correct near-wall integration is guaranteed by  $y^+ < 1$  and

15-20 elements inside the boundary layer on all viscous surfaces. An overview of the element size and distribution around the pedestal leading edge can be seen in Fig.2.

## RESULTS

### Inflow conditions

With the aim of providing the correct boundary conditions for the numerical simulations, the inlet flow was measured along the two symmetry planes of the entry rectangular section. Profiles of the time-averaged U velocity component have been extracted along Pin\_xy and Pin\_xz and plotted in Fig.3. The stream-wise velocity profile in the xy1 plane (Fig.3(a)) is slightly unbalanced due to the blockage effect of the redirecting wall located at the leading side of the channel ( $Y = 2.31D = 120$  [mm]). The

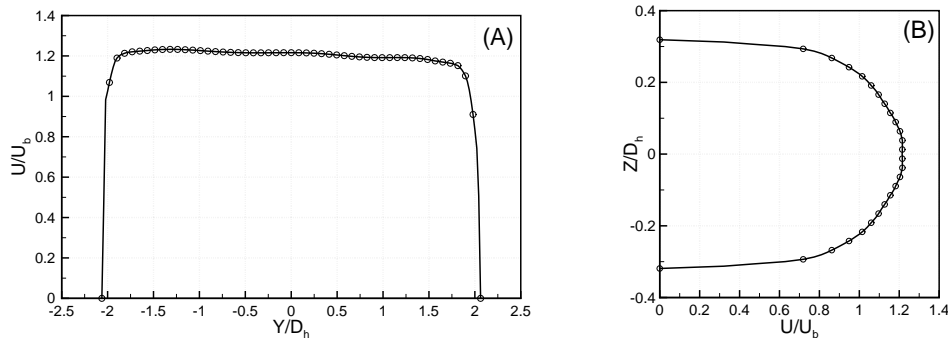


**FIGURE 3. Time-averaged stream-wise velocity profiles extracted in the inlet duct along lines Pin\_xy (a) and Pin\_xz (b).**

velocity profile along the Z axis is typical of a turbulent but not fully developed channel flow, in view of the short entry length of channel. As shown by the reported velocity profiles, the honey-comb at the channel inlet section prevents the flow to separate.

These profiles are the basis to impose the correct inlet boundary conditions for the numerical analysis: 2D interpolation was performed to reconstruct normal velocity for every inlet boundary face following Eq.1.

$$U_{in}(y,z) = U_{Pin_{xz}}(z) \cdot U_{Pin_{xy}}(y) / U_{Pin_{xy}}(0). \quad (1)$$

The resulting bulk velocity is about 5.2 [m/s].

Moreover, measurements also provide turbulent fluctuation levels as shown in Tab.1 with reference to the bulk flow.

**TABLE 1. Normalized RMS fluctuating velocity values at Pin\_yz y=z=0**

$U_{RMS}/U_b$	$V_{RMS}/U_b$	$W_{RMS}/U_b$
4.2%	2.9%	2.7%

Such values could not be directly imposed for the numerical calculations since RANS implies turbulence isotropy thus were converted into a specified turbulent intensity for the CFD runs:

$$Tu = \sqrt{\frac{2}{3} \cdot k / U_b^2} = \sqrt{\frac{1}{3} (U_{RMS}^2 + V_{RMS}^2 + W_{RMS}^2) / U_b^2} = 3.33\%. \quad (2)$$

Dissipation length, necessary to close the boundary conditions for a two equation model, was instead estimated from the honey-comb filter spacing at the inlet section to be 4 [mm].

### Velocity maps

In order to provide a first comparison between experimental results and numerical predictions, Figs.4 and 5 report the in-plane time averaged data in terms of streamtracers path and contour plots of the velocity magnitude on xy1 and xy2 planes, respectively. The seeding to generate the experimental and numerical streamtracers is clearly not equivalent, thus these lines should only be used as a support in the visualization. For sake of brevity, only data for the open tip configuration are presented.

From a qualitative point of view, all the main flow field characteristics are well captured by the CFD computations. The mean velocity of the flow inside the duct reduces gradually along the radial direction in view of the constant flow discharge along the

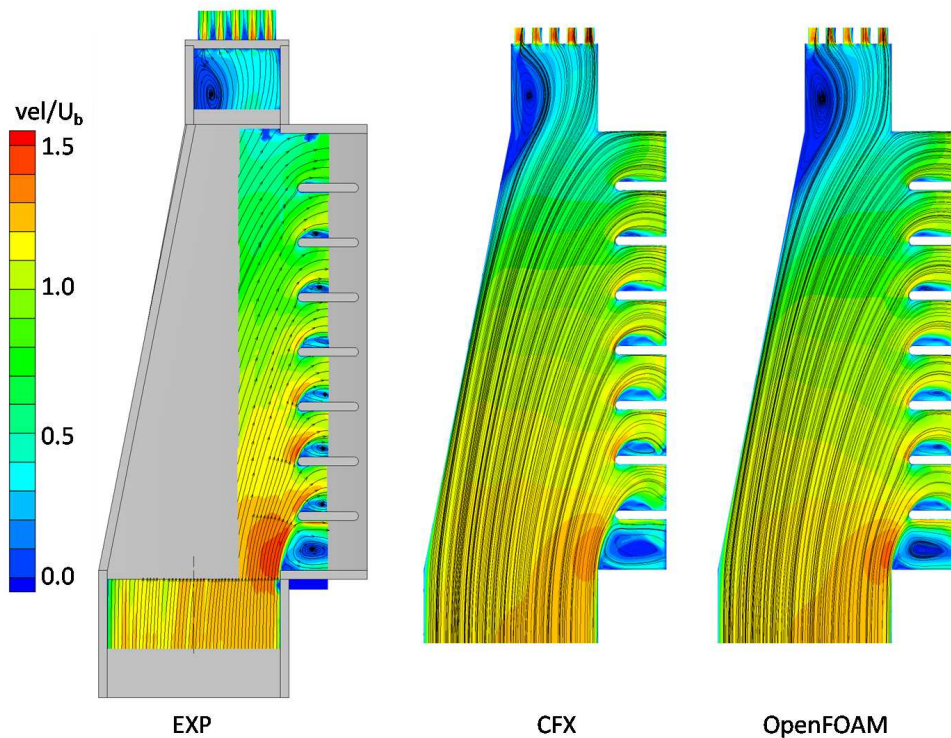


**FIGURE 4. Overview of the velocity field in plane xy1 - open tip case**

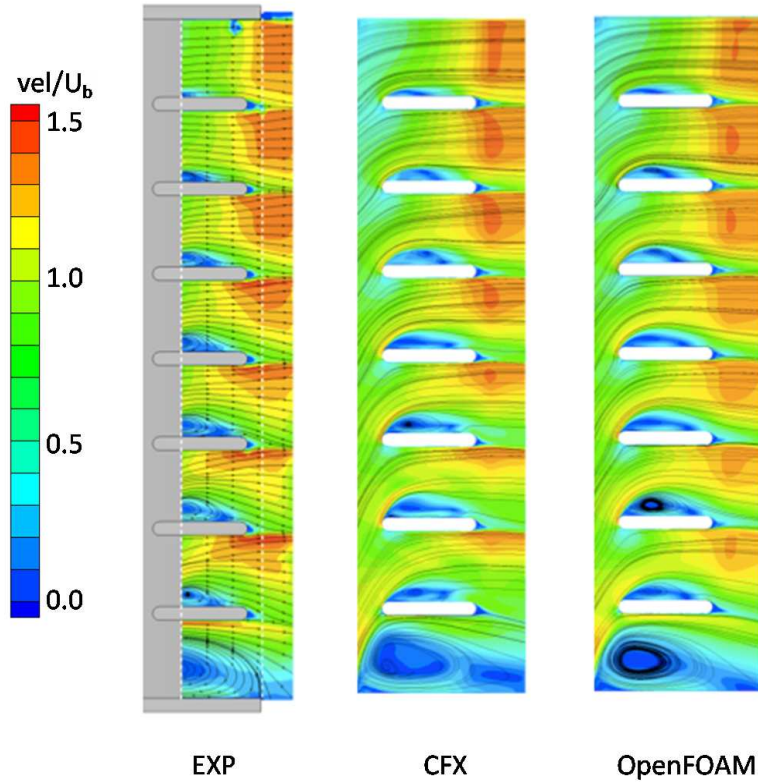


FIGURE 5. Trailing Edge detail of the velocity field in plane xy2 - open tip case

trailing edge. Two large recirculation bubbles are clearly evident, the first one at the tip region just after the end of the redirecting wall, the second one in the first discharge passage close to the hub. Smaller recirculation bubbles are present downstream of each pedestal and show decreasing dimension at increasing radii. With particular reference to Fig.5, both experiments and computations show that each discharge passage is characterized by strong velocity gradients in the X-direction with decreasing intensity moving from hub to tip. Indeed, as the flow approaches the tip region, it becomes more axially oriented (i.e. Y axis direction) and the incidence angle with respect to the obstacles reduces. Consequently the separation structures produced at the pedestal pressure and suction sides are narrower, leading to a more uniform flow.

### Velocity profiles

To better quantitatively assess the agreement of the CFD prediction with the experimental results for both open and closed tip configurations, velocity profiles were extracted on the lines Pte1-Pte3 specified in Fig.1-B.

The first line to be investigated is Pte1, corresponding to the entrance of the trailing edge duct in plane xy1. Incidence an-

gle ( $\alpha$ ) of the flow with respect to the Y-direction is plotted in Fig.6. For the open tip case, the flow angle relative to the pedestal chord decreases moving towards higher radii, according with the reduction of the recirculation bubble noticed from the velocity maps. Almost identical values and trend of the incidence angle are found for the closed tip case. In the first inter-pedestals duct the recirculation bubble is highlighted by the change in sign corresponding to an inversion of the axial velocity. Its extension is slightly over-predicted by both the CFD codes for both channel configurations, with OpenFOAM<sup>®</sup> predictions lowering such gap.

The different trend predicted by OpenFOAM<sup>®</sup> for the closed tip condition, i.e. no spikes in changing incidence orientation, is due to a different orientation of the secondary vortex developing behind the trailing edge duct corner. From the second to the sixth inter-pedestals passage, the agreement among the CFD codes and the experiments is almost total for both tip conditions. Only for the closed tip case the numerical values result to be slightly in over-prediction for the last two passages, showing less variability with the tip condition. The concordance obtained for these data is certainly a key issue to succeed in well predicting the recirculation bubbles on the pedestal suction side, mispredicting

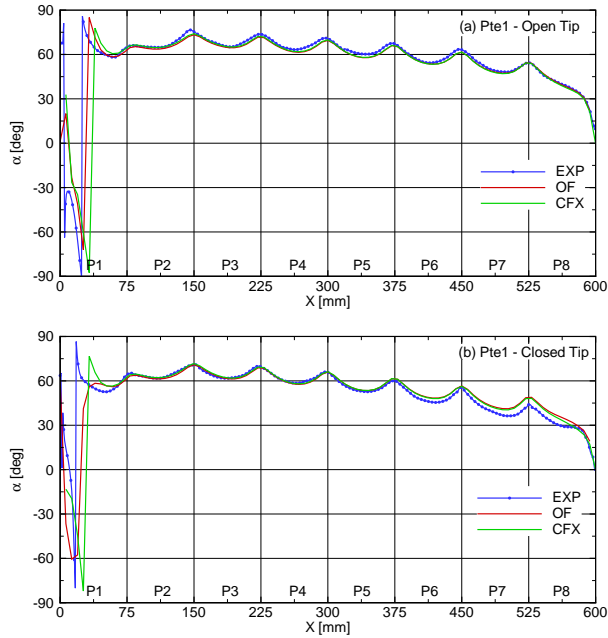


**FIGURE 6. Incidence angle at Pte1**

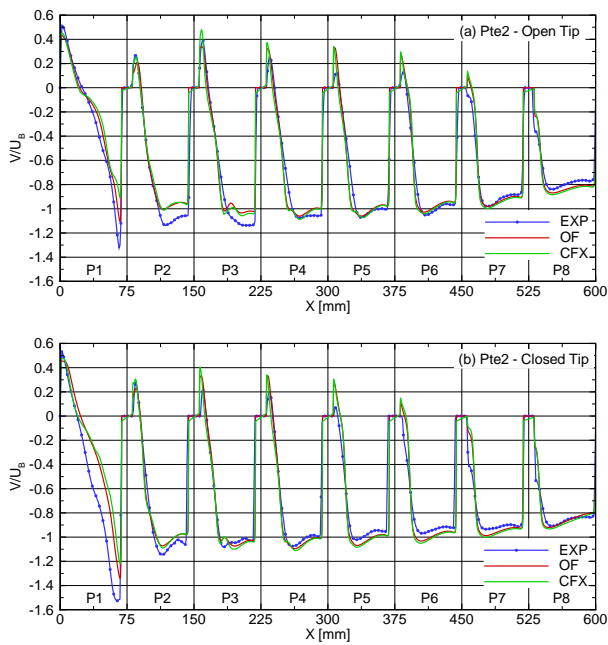


**FIGURE 7. Axial velocity profiles at Pte2**

the incidence on the leading edge would in fact affect the interpedestals duct loading conditions.

Figure 7 reports the axial velocity values for open and closed tip conditions along line Pte2, located around mid-pedestal posi-

tion. The experimental data show that the different tip conditions have their most evident effect on the first passage. The variation of the tip conditions from open to closed tip will turn in an augmented mass flow to be discharged along the trailing edge. Where the flow is already well aligned in Y-direction (i.e. the passage closest to the tip), this results just in a augmentation of the velocity. On the contrary, where the flow is mostly separated (i.e. the passage closest to the hub) this effect will lead also to a significant reduction of the recirculating bubble extension. The comparison with the numerical results show an overall good agreement. The more pronounced discrepancies are found only in the first passage, where the two codes predict a bigger separation and a lower peak velocity. This would suggest a lower mass flow rate swallowed at lower radii, as confirmed by the air splits analysis reported in the following section. These differences are more pronounced for the closed tip configuration. For the other passages, the numerics correctly predict the near pedestal flow with a well captured extension of the separated regions. Only small discrepancies with respect to the experiments can be observed for the peak velocities in the central portion of the ducts.

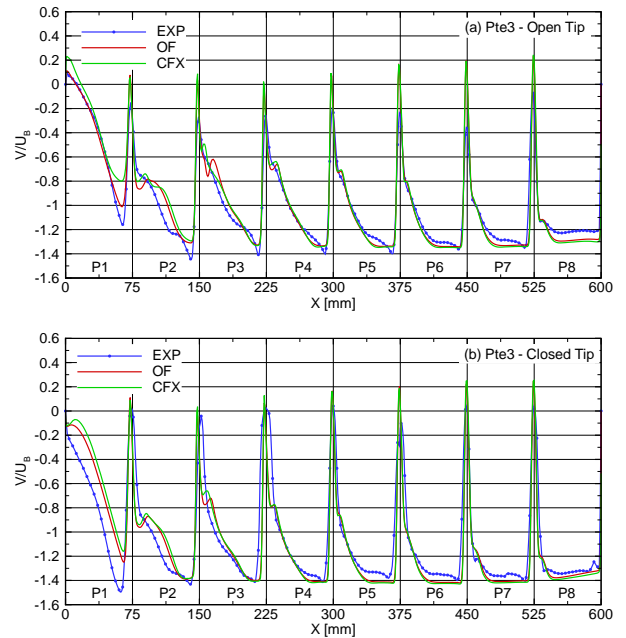


**FIGURE 8. Axial velocity profiles at Pte3**

Looking in Fig.8 at equivalent profiles extracted along Pte3, near the pedestal trailing edge, for both the open and closed tip cases, a deficiency in predicting the near pressure side pedestal zone can be highlighted. In these positions, the experiments

reports a sharp velocity peak, such behaviour is not reproduced by computations that predict a more diffused high velocity zone with a flatter profile. For the open tip configuration, in the first inter-pedestals passage OpenFOAM® predictions reproduce quite well the extension of the recirculation bubble, whilst CFX® sees a more intense flux inversion with respect to experiments. For closed tip both numerical solutions and experiments reveal no recirculation, lower velocity levels are presented by the numerics.

It has to be noticed that the differences found in the narrow region of the pedestals' wake where the numerics in all cases predict a velocity inversion (see Fig.8) has to be ascribed to the spatial resolution of the experimental data, not high enough to resolve such small flow structures.

### Air splits

Even though for numerical predictions the evaluation of the mass flow fraction discharged at the tip and by each inter-pedestals duct can be easily computed by means of surface integrals on selected planes since data are available at any grid point, this is not the case for the experimental values that are available only at specific positions. In order to evaluate the mass flow fraction discharged at the tip with respect to the total amount entering the channel, stream wise velocity profiles were obtained also from velocity fields measured in xz-F1,...xz-F5 planes (see Fig.1-B) and not reported for brevity. These data, together with the profile Ptip extracted at X=730 [mm] from plane xy1 (see Fig.1-B), allowed to reconstruct the stream wise velocity maps over the jets cross section which have been numerically integrated to compute the mass flow fraction discharged at the tip section  $q_{tip}$ . Same procedure was applied to the inlet section in order to evaluate  $q_{in}$ .

Concerning the mass flow through the trailing edge, a precise estimation of this value could be possible only if the V velocity distribution along the Z axis was known. Since this information is not available in the present experimental data base, an estimation of the mass flow was obtained as follows. The V velocity profiles at positions Pte1, Pte2 and Pte3 have been integrated along the X coordinate separately over the eight inter-pedestals passages and the results have been normalized with respect to their overall integral values. Only for the open tip case, a scale factor of 0.901 has been applied to the integrals in order to take into account for the mass flow discharged at the tip section (which is actually 0.099 of  $q_{in}$ ). The coherence of the results obtained by the described procedure once applied to the three velocity profiles Pte1, Pte2 and Pte3 (i.e at very different locations inside the channel) suggests that they can be considered a reliable estimation of the mass flow split, despite the strong three-dimensional character of the inter-pedestals flow. An averaged value of the air-split was finally extracted and compared with numerical results.

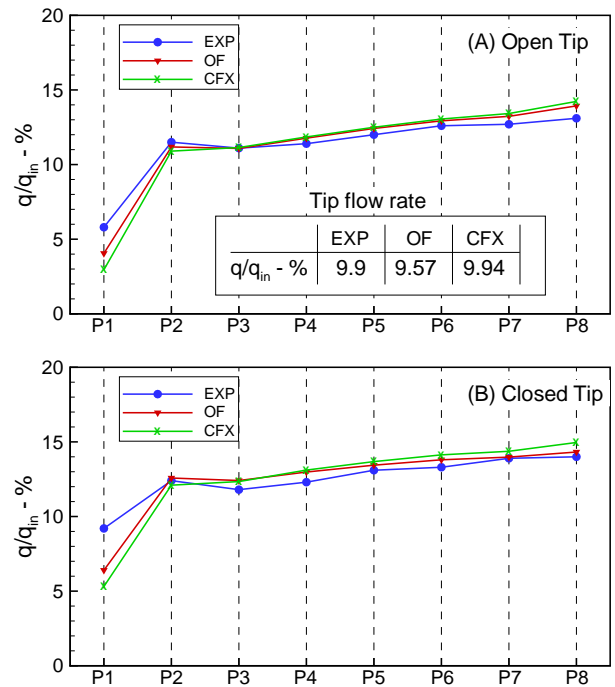


**FIGURE 9. Inter-pedestals mass flow rate distribution**

Figure 9 reports the air splits for the various inter-pedestals ducts. Those data demonstrate the correct design of the channel: the combined effect of redirecting wall and pedestals guarantee an almost uniform flow along the trailing edge, with a slightly increasing mass of gas discharged at higher radii and a mean value slightly above 10% of  $q_{in}$ . Only in the first inter-pedestals passage, because of the blockage effect imposed by the large recirculation previously commented, less than half coolant flow rate is swallowed.

Results of both numerical predictions and measurements agree well in confirming these findings. The under-prediction of the mass flow rate elaborated by the first passage is coherent with the higher extension of the recirculation found by the numerics, as previously commented.

For the open tip configuration, both experiments and numerics converge to the same value of mass flow rate exhausted from the tip section, i.e. about 10% of  $q_{in}$ .

### 3D inter-pedestals flow structures

This last section provides an analysis of the three-dimensional flow structures that develop inside the inter-pedestals passages in order to complete the flow field analysis and check the capability of the tested CFD codes to predict correctly even such complex flow features. The analysis is

conducted inside passage P4 (see Fig.1-B) by means of the experimental data acquired in the xy3, xy4, xz1 and xz2 planes, Figs.10. In view of the above commented results that show no significant differences in the flow structures at the two tip mass flow rates only data about the open tip condition are presented.

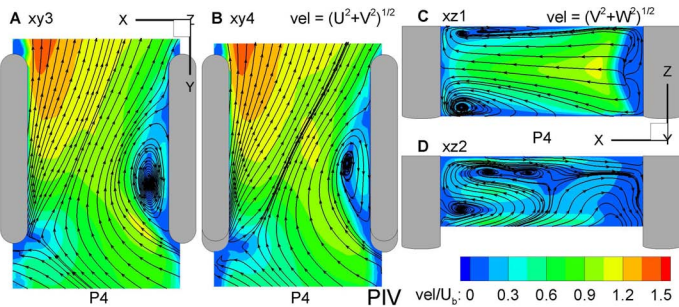


**FIGURE 10. Detail of the 3D inter-pedestals flow structures - PIV data - open tip case.**

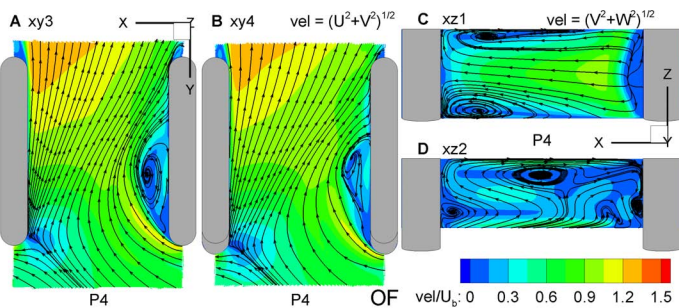


**FIGURE 11. Detail of the 3D inter-pedestals flow structures - CFD-OF solution - open tip case.**

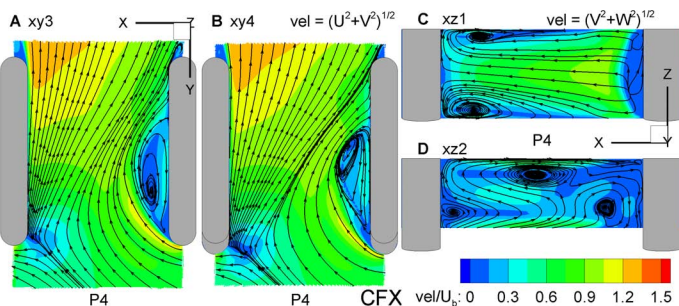


**FIGURE 12. Detail of the 3D inter-pedestals flow structures - CFD-CFX solution - open tip case.**

The time averaged stream-tracers path in planes xy3 and xy4 (Figs.10-A-B) indicates the existence of horse-shoe vortices on the upstream face of the 4th pedestal generated by the deviation of the approaching boundary layers. The dimensions of these junction flows can be depicted by the stream-tracers path in plane xz1 (Fig.10-C). On the blade suction side, corresponding to the inclined side of the duct with  $Z < 0$ , the horse-shoe vortex appears has a single structure that extends approximately over half of the channel height.

On the contrary, on the blade pressure side ( $Z > 0$ ) the horse-shoe is made of two vortex cells with an over-all dimension smaller with respect to the one on the other channel side. However, the contour plot of the in-plane velocity in Fig.10-C suggests that the inter-pedestals flow structure can still be considered fairly symmetric with respect to the X axis. On pedestal suction side the flow is dominated by the separation bubble and no clear imprint of the horse-shoe vortex is highlighted, streamlines show that a motion from pedestal midspan towards the endwalls is present. Moving towards the channel trailing edge, the time averaged flow structure (see Fig.10-D) is further complicated by the flow acceleration imposed by the narrowing of the channel. The horse-shoe structures appear bigger in size and air exchange between pedestal pressure and suction sides takes place. Similar flow features have been observed also in the measurements conducted in the other trailing edge exhaust ducts, the only difference consists in a reduction of the separated flow structures downstream of each pedestal when moving towards the blade tip, as already commented in Figs.4 and 5.

The comparison with the numerical results presented in Figs.11 and 12 shows that both the tested CFD codes provide a good prediction of the complex inter-pedestals flow structures. Both size and position of the main vortical structures are well captured, the only significant discrepancy can be observed in a different evolution of the horse-shoe vortices that develop on the blade pressure side ( $Z > 0$ ). In particular in plane xz2, located around mid-pedestal position, both numerical codes predict only one vortex cell localized around passage centerline.

## CONCLUSIONS

The flow field inside a wedge shaped trailing edge cooling device provided with seven pedestals was investigated. A mixed axial-radial flow was developed by means of a radial inlet and a redirecting device. Influence of tip discharge condition was assessed considering two different geometries: a closed channel and a five circular hole top. Reference flow conditions were imposed at  $Re = 20000$ .

Two-dimensional PIV measurements were performed on selected planes in order to analyze the overall flow field structure. A high resolution set of measurements was dedicated to the investigation of the complex three-dimensional structures in the inter-pedestals passages. Steady state RANS CFD analysis was also

performed exploiting the commercial code Ansys®CFX® and the open source toolbox OpenFOAM®.

Results are reported in terms of velocity maps from which data are extracted at selected lines corresponding to the entrance of the trailing edge duct, the mid pedestal section and the trailing edge plane. Furthermore the coolant mass flow rate inside each passage was evaluated to assess the working conditions of each channel.

A recirculation bubble is developing on the suction side of each pedestal with decreasing extension at higher radii, vice versa an accelerating flow is found on the pressure side where horse-shoe vortices develop in the near wall regions. The outflow at the trailing edge is almost completely axial for the inter-pedestals passage close to the blade hub for which a wide recirculation is affecting the discharge. For the open tip condition a 10% mass flow rate discharged at the tip was found. The closed tip configuration, revealed almost the same features as the open one.

Steady state RANS analysis provided, for the investigated cases, confident predictions of the flow field with a very good agreement with the experimental data. The main discrepancies were found in the prediction of the extension of the separation bubbles on the first inter-pedestals passage. Both the numerical codes provided also reliable simulations of the complex three-dimensional flow structure within the inter-pedestals passages. Key issues in obtaining such concordance with experiments were found to be the availability of precise boundary conditions and the grid refinement around the pedestal leading edge.

## ACKNOWLEDGMENTS

The present work has been supported by the Italian Ministry of University and Research (MiUR). The authors would like to acknowledge L. Andrei, C. Mucignat and PhD R. Da Soghe for the help given.

## REFERENCES

- [1] Taslim, M., Li, T., and Spring, S., 1998. "Measurements of heat transfer coefficients in rib-roughened trailing-edge cavities with crossover jets". *Proceedings of ASME Turbo Expo 1998: Power for Land, Sea and Air*(98-GT-435).
- [2] Armellini, A., Coletti, F., Arts, T., and Scholtes, C., 2010. "Aero-thermal investigation of a rib-roughened trailing edge channel with crossing-jets. Part I: flow field analysis". *Journal of Turbomachinery*, **131**(1), pp. 011009–1–9.
- [3] Coletti, F., Armellini, A., Arts, T., and Scholtes, C., 2008. "Aero-thermal investigation of a rib-roughened trailing edge channel with crossing-jets. Part II: heat transfer analysis". *Proceedings of ASME Turbo Expo 2008: Power for Land, Sea and Air*(GT2008-50695).
- [4] Coletti, F., Manfredi, S., and Arts, T., 2010. "Experimental investigation of conjugate heat-transfer in rib-roughened trailing edge channel with crossing-jets". *Proceedings of ASME Turbo Expo 2010: Power for Land, Sea and Air*(GT2010-22432).
- [5] Choi, J., Mhetras, S., Han, J., Lau, S., and Rudolph, R., 2008. "Film cooling and heat transfer on two cutback trailing edge models with internal perforated blockages". *Journal of Heat Transfer*, **130**, pp. 012201–1–012201–13.
- [6] Cakan, M., and Taslim, M., 2007. "Experimental and numerical study of mass/heat on an airfoil trailing-edge slots and lands". *Journal of Turbomachinery*, **129**, pp. 281–293.
- [7] Facchini, B., Simonetti, F., and Tarchi, L., 2009. "Experimental investigation of turning flow effects on innovative trailing edge cooling configurations with enlarged pedestals and square or semicircular ribs". *Proceedings of ASME Turbo Expo 2009: Power for Land, Sea and Air*(GT2009-59925).
- [8] Facchini, B., Simonetti, F., and Tarchi, L., 2009. "Experimental investigation of turning flow effects on innovative trailing edge cooling configurations based on circular and oblong pin fins". *Proceedings of 8th European Turbomachinery Conference*(170).
- [9] Bianchini, C., Facchini, B., Simonetti, F., Tarchi, L., and Zecchi, S., 2010. "Numerical and experimental investigation of turning flow effects on innovative pin fin arrangements for trailing edge cooling configurations". *Proceedings of ASME Turbo Expo 2010: Power for Land, Sea and Air*(GT2010-23536).
- [10] Bianchini, C., Bonanni, L., Carcasci, C., Facchini, B., and Tarchi, L., 2010. "Experimental survey on heat transfer in an internal channel of a trailing edge cooling system". *65 Associazione Termotecnica Italiana National Congress*.
- [11] Bianchini, C., Andreini, A., and Facchini, B., 2011. "Numerical analysis of flow and heat transfer in a trailing edge cooling duct in stationary and rotating conditions". *Proceedings of 9th European Turbomachinery Conference*(170).
- [12] Kline, S. J., and McClintok, F. A., 1953. "Describing Uncertainties in Single Sample Experiments". *Mechanical Engineering Journal*, **75**(1), January, pp. 3–8.
- [13] PIVview2C/3C User Manual Version 3.0.6. Tech. rep., PivTec GmbH.
- [14] Willert, C., Raffel, M., Wereley, S., and Kompenhans, J., 2007. *Particle image velocimetry: a practical guide*. Springer-Verlag Berlin Heidelberg.
- [15] Casarsa, L., and Giannattasio, P., 2008. "Three-dimensional features of the turbulent flow through a planar sudden expansion". *Physics of Fluids*, **20**, pp. 015103–1–015103–15.
- [16] ANSYS CFX-11.0 User Guide. Tech. rep., ANSYS Inc. 2007.

- [17] OpenFOAM Programmers Guide. Tech. rep., OpenCFD Limited.
- [18] OpenFOAM User Guide. Tech. rep., OpenCFD Limited.
- [19] Andreini, A., Bianchini, C., Facchini, B., and Mangani, L., 2007. “Development and validation of a C++ object oriented CFD code for heat transfer analysis”. *ASME-JSME 2007 Thermal Engineering and Summer Heat Transfer Conference*(AJ-1266).
- [20] Jasak, H., 1996. “Error analysis and estimation for the finite volume method with applications to fluid flows”. PhD thesis, Imperial College of Science, Technology and Medicine.
- [21] Menter, F., Thomas, E., and Vieser, W., 2003. “Heat transfer predictions based on two-equation turbulence models”. *ASME-JSME 2003 Thermal Engineering Joint Conference*.
- [22] Hanjalic, K., and Popovac, M., 2007. “Compound wall treatment for RANS computation of complex turbulent flows and heat transfer”. *Flow, Turbulence and Combustion*, **78**(2).
- [23] Mangani, L., and Andreini, A., 2008. “Application of an object oriented CFD code to heat transfer analysis”. *Proceedings of ASME Turbo Expo 2008: Power for Land, Sea and Air*(GT2008-5111).